


RESEARCH ARTICLE

Validation of the *Aeolus* L2B Rayleigh winds and ECMWF short-range forecasts in the upper troposphere and lower stratosphere using Loon super pressure balloon observations

Sebastian Bley^{1,2}  | Michael Rennie³ | Nedjeljka Žagar⁴ | Montserrat Pinol Sole⁵ | Anne Grete Straume⁵ | James Antifaev⁶ | Salvatore Candido⁶ | Robert Carver⁶ | Thorsten Fehr⁵ | Jonas von Bismarck¹ | Anja Hünnerbein² | Hartwig Deneke²

¹ESA-ESRIN, Centre for Earth Observation, Frascati,

²Leibniz Institute for Tropospheric Research, Leipzig, Germany

³ECMWF, European Centre for Medium-Range Weather Forecasts, Reading, UK

⁴Meteorological Institute, Universität Hamburg, Hamburg, Germany

⁵ESA-ESTEC, European Space Research and Technology Centre, Noordwijk, the Netherlands

⁶Loon, Mountain View, California, USA

Correspondence

Sebastian Bley, Leibniz Institute for Tropospheric Research, Permoserstrasse 15, 04318 Leipzig, Germany.
Email: sebastian.bley@tropos.de

Abstract

The novel *Aeolus* satellite, which carries the first Doppler wind lidar providing profiles of horizontal line-of-sight (HLOS) winds, addresses a significant gap in direct wind observations in the global observing system. The gap is particularly critical in the tropical upper troposphere and lower stratosphere (UTLS). This article validates the *Aeolus* Rayleigh-clear wind product and short-range forecasts of the European Centre for Medium-Range Weather Forecasts (ECMWF) with highly accurate winds from the Loon super pressure balloon network at altitudes between 16 and 20 km. Data from 229 individual balloon flights are analysed, applying a collocation criterion of 2 hr and 200 km. The comparison of *Aeolus* and Loon data shows systematic and random errors of -0.31 and $6.37 \text{ m}\cdot\text{s}^{-1}$, respectively, for the *Aeolus* Rayleigh-clear winds. The horizontal representativeness error of *Aeolus* HLOS winds (nearly the zonal wind component) in the UTLS ranges from 0.6 – $1.1 \text{ m}\cdot\text{s}^{-1}$ depending on the altitude. The comparison of *Aeolus* and Loon datasets against ECMWF model forecasts suggests that the model systematically underestimates the HLOS winds in the tropical UTLS by about $1 \text{ m}\cdot\text{s}^{-1}$. While *Aeolus* winds are currently considered as point winds by the ECMWF data assimilation system, the results of the present study demonstrate the need for a more realistic HLOS wind observation operator for assimilating *Aeolus* winds.

KEYWORDS

Aeolus, data assimilation, ECMWF forecasts, HLOS winds, Loon, super pressure balloon observations, systematic and random errors

1 | INTRODUCTION

Atmospheric winds simulated by numerical weather prediction (NWP) models are by definition uncertain, with uncertainties dependent on the flow and increasing with the forecast length. The uncertainties arise due to inaccurate observations that are used to prepare the initial state (analysis) for the model forecasts, due to model errors and the chaotic nature of the simulated flow as well as combinations of these factors. The present study addresses the uncertainties in the analyses and short-range forecasts that are known to be largest in the tropical upper troposphere and lower stratosphere (UTLS: e.g., Žagar *et al.*, 2013; Rennie, 2016; Žagar, 2017). The uncertainties are commonly estimated by operational ensemble data assimilation and ensemble prediction systems such as the Integrated Forecasting System (IFS) of the European Centre for Medium-Range Weather Forecasts (ECMWF). However, a reliable quantification of tropical analysis and forecast uncertainties represents a major challenge, since direct wind observations in the UTLS are relatively sparse. Furthermore, uncertainties estimated by operational NWP model ensembles are influenced by data assimilation methodology and by the method used to prepare the initial perturbations for the ensemble forecasts.

The academic and NWP communities have long argued for a global coverage of wind-profile measurements for NWP and a better characterization of the climate system (Baker *et al.*, 2014). The existing global observing system includes observations of wind profiles from radiosondes, aircraft data, or wind profilers, but they are mostly concentrated over the Northern Hemisphere and Extratropics. Traditional satellite-based direct wind observations are limited to the cloud-top layer for atmospheric motion vectors (AMVs), or to the Earth's surface for scatterometers. AMVs provide single-layer winds on a global basis, but introduce significant uncertainties, particularly in the assignment of the corresponding altitude (e.g., Borde and Arriaga, 2004; Velden and Bedka, 2009; Salonen *et al.*, 2012).

A large step ahead in global wind measurements was made with the approval and development of the European Space Agency (ESA) wind mission *Aeolus* (Stoffelen *et al.*, 2005), which was launched on August 22, 2018. ESA's Earth Explorer *Aeolus* carries a single payload, the Atmospheric Laser Doppler Instrument (ALADIN) (e.g., ESA, 1999; Stoffelen *et al.*, 2005; Reitebuch, 2012). ALADIN is the first ever Doppler wind lidar in space, providing profiles of the wind component along its horizontal line-of-sight (HLOS) direction, from the Earth's surface or from the top of optically thick clouds up to about 30 km on a global scale.

One of the primary objectives of the *Aeolus* mission is to improve global medium-range weather forecasts by assimilating HLOS wind profiles in near-real time (e.g., Marseille *et al.*, 2008; Horányi *et al.*, 2015a; Horányi *et al.*, 2015b; Šavli *et al.*, 2018; Rennie and Isaksen, 2020). The ECMWF started their operational assimilation of the *Aeolus* HLOS winds in January 2020 following a major effort in bias reduction (Rennie *et al.*, 2021). Since then, the *Aeolus* wind profiles have been shown to be useful for NWP analyses and forecasts not only at ECMWF (Rennie and Isaksen, 2020) but also at other global NWP centres (e.g., Pourret *et al.*, 2021; Garrett *et al.*, 2022; Laroche and St-James, 2022). All the centres agree that the largest positive impact of *Aeolus*'s HLOS winds is found in the Tropics and particularly in the UTLS.

Dynamical processes in the tropical UTLS include both vertically and horizontally propagating large-scale equatorial waves and a spectrum of small-scale gravity waves superimposed on low-frequency variability such as the Madden–Julian oscillation and the quasibiennial oscillation. Wave properties are difficult to characterize, due to their complex coupling to convection and model deficiencies in representing processes that substantially take place at the cloud scale. Wind perturbations of the equatorial waves derived from temperature observations suffer from uncertainties in the assumptions involved in wave filtering (Stephan *et al.*, 2021). In particular, wind shear in the tropopause layer is difficult to represent correctly in analyses due to the smoothing effect of data assimilation (Podglajen *et al.*, 2014) and model errors. The first study of the impact of *Aeolus* HLOS winds in the UTLS by Žagar *et al.* (2021) showed that the *Aeolus* wind profiles provide unique observations of the wind shear within the UTLS region, which is crucial for the accuracy of stratospheric forecasts.

Another observing system with the potential to partially fill the gap in global wind observations is super pressure balloons. Such balloons provide unique information about atmospheric dynamics from short-range gravity waves to long planetary waves as demonstrated in the framework of the Stratéole project (Hertzog *et al.*, 2007). Super pressure balloons can be considered as quasi-Lagrangian tracers, as their horizontal motions are nearly identical to those of the surrounding air mass (Haase *et al.*, 2020), which allows us to infer the horizontal wind speed with an accuracy better than 0.1 m s^{-1} (Hertzog *et al.*, 2007). Haase *et al.* (2018) showed that super pressure balloons can contribute remarkably to the quantification of uncertainties and model errors. Between November 2019 and February 2020, the Stratéole-2 project launched eight super pressure balloons in the tropical lower stratosphere (Hertzog and Plougonven, 2021). The campaign aimed at testing new technologies in order to study and

understand better the climate processes in the tropical tropopause layer, which forms the gateway between the troposphere and the stratosphere. The Stratéole-2 observations were also intended for the validation of the *Aeolus* wind products (Haase *et al.*, 2020). Further balloons are expected to be launched in 2022 and 2024.

Another project with a network of super pressure balloons is Loon (Rhodes and Candido, 2021). The Loon project was designed to provide internet connectivity to remote regions. The Loon balloons fly in the tropical tropopause layer (TTL) at approximately 16–20 km altitude. Through their onboard Global Positioning System (GPS) sensor, the zonal and meridional wind speed can be derived from the balloon platform drift with a high accuracy, having wind biases of less than $0.23 \text{ m}\cdot\text{s}^{-1}$ (Friedrich *et al.*, 2017).

This article makes use of the Loon measurements during a large part of the *Aeolus* mission in the period from 2018–2020, which allows the analysis of long-term biases and trends of the *Aeolus* wind products. This study presents the first comparison of the *Aeolus* Level 2B products and the ECMWF forecasts based on the assimilated *Aeolus* winds with the wind observations from the Loon network. Thanks to the high accuracy of the Loon winds, they can serve as an independent dataset to evaluate the *Aeolus* HLOS and the ECMWF model winds. This provides a unique quantification of the uncertainty of the NWP system in the critical UTLS region of the Tropics with most of the Loon balloons.

The article is structured as follows. Section 2 introduces the three datasets and describes the validation methodology. The results in terms of systematic and random errors are presented in Section 3. The article closes with a discussion of the results in Section 4 and conclusions in Section 5.

2 | DATA AND METHODOLOGY

2.1 | *Aeolus* wind product

The *Aeolus* Level 2B (L2B) wind product contains profiles of the HLOS wind speed along the satellite's measurement track (Rennie and Isaksen, 2020). The *Aeolus* satellite orbits the Earth in a polar sun-synchronous dawn–dusk orbit (97° inclination and 18:00 local Equator-crossing time of the orbit ascending node), at an average altitude of 320 km above the surface with a repeat cycle of 7 days. Its ALADIN instrument emits short laser pulses at a frequency of 50 Hz, at a wavelength of 355 nm under a 35° off-nadir angle away from the Sun perpendicular to the flight track, in order to minimize the contribution of solar background and to avoid contamination of

the Doppler measurements with the speed of the platform. The backscattered light from the atmosphere is collected by a telescope and reflected to the Rayleigh and Mie channels of the receiver unit, where the wind speed is derived from the Doppler frequency shift (Reitebuch, 2012; Lux *et al.*, 2020). The detector unit with an accumulation charge-coupled device (CCD) has 24 vertical range bins, which divide the atmosphere into layers or boxes with varying distances and times (e.g., Stoffelen *et al.*, 2005; Straume *et al.*, 2020). Wind measurements can be obtained between the Earth's surface and 30 km, while the vertical resolution can be adjusted flexibly between 250 m and 2 km depending on the objective and application (e.g., Reitebuch, 2012; Lux *et al.*, 2020).

One *Aeolus* measurement corresponds to a horizontal length of approximately 3 km in the along-track direction, which defines the accumulation of the backscattered signal of 18 laser pulses. The 3-km measurements are classified into clear/cloudy features before they are accumulated further to a defined maximum horizontal size. The product is classified into Rayleigh–clear winds, indicating observations in clear air (i.e., without aerosols and water/ice clouds) and Mie–cloudy winds, indicating winds retrieved from aerosol or cloud particle backscatter (Tan *et al.*, 2008; Rennie *et al.*, 2020, 2021; Witschas *et al.*, 2020). For a Rayleigh–clear wind observation, up to 30 measurements are accumulated along the measurement track (30 measurements are accumulated only if all of them are labelled as clear air, fewer than 30 if some of the features at measurement scale are labelled as cloudy), which corresponds to a horizontal resolution of 87 km (Lux *et al.*, 2020; Rennie *et al.*, 2020, 2021). The actual Rayleigh–clear wind speed is given at the horizontal and vertical centre of gravity of the observations. The product also includes geolocation information about the top/bottom of the vertical range bin and the start/end of the horizontal 87-km box in case more complex nonlinear averaging is required.

Only *Aeolus* L2B Rayleigh–clear winds are considered for the comparison against Loon and ECMWF winds, because clouds and aerosol are rarely present in the UTLS. The Rayleigh channel aims for a pure molecular signal, however it can be affected by Mie contamination, which would cause biases in the retrieved winds. This issue is solved by classification of clear and cloudy measurements before accumulation to the observation scale. The L2B processor also provides a Rayleigh–cloudy wind observation, including the cloudy features measured by the Rayleigh channel, which is of poorer quality and not considered for this study.

To correct for temperature and pressure effects in the Rayleigh wind retrieval, profiles of temperature and pressure are used from the ECMWF model forecast (e.g., Dabas *et al.*, 2008; Šavli *et al.*, 2021). These data are included

in the auxiliary meteorological data product (AUX_MET), which is described further in Section 2.3. The *Aeolus* L2B product also includes the wind result validity flag, Rayleigh–clear wind-error estimate, and model reference wind from the ECMWF model. The Rayleigh–clear error estimate is derived from the signal-to-noise level and the temperature and pressure sensitivity of the Rayleigh channel and thus accounts mainly for the instrument noise (Tan *et al.*, 2008; Rennie *et al.*, 2020). In this study, *Aeolus* winds are used only if the confidence flag is set to “valid”. Furthermore, *Aeolus* wind measurements for which the Rayleigh–clear error estimate is larger than $8 \text{ m}\cdot\text{s}^{-1}$ are rejected with the aim of removing occasional gross errors, which are more common for very low signals. The applied error threshold has been recommended by the *Aeolus* Data Innovation and Science Cluster (DISC) as an additional quality control filter for wind validation activities (e.g., Stoffelen *et al.*, 2019; Rennie and Isaksen, 2020; Reitebuch *et al.*, 2020a).

For a consistent comparison between *Aeolus* measurements and datasets from external sources (e.g., an NWP model or independent observations), the *Aeolus* observational geometry needs to be taken into account (Lux *et al.*, 2020). The Loon balloon observations and the ECMWF model provide both the zonal and meridional wind components, u and v respectively, which have to be converted to the HLOS wind component v_{HLOS} using the azimuth angle ϕ of the position of the collocated *Aeolus* observation:

$$v_{\text{HLOS}} = -u \sin(\phi) - v \cos(\phi). \quad (1)$$

Because the direction of v_{HLOS} points perpendicularly to the *Aeolus* track, it observes mainly the zonal wind component, except near the poles. If v_{HLOS} is positive, the wind blows away from the instrument, while negative values indicate winds that are blowing towards the instrument. As a consequence, westerly winds are positive for ascending orbits and negative for descending orbits. For this study, we multiply winds for descending orbits by -1 to obtain always positive values for westerly and negative values for easterly winds. In the *Aeolus* L2B products, the vertical wind component is assumed to be negligible over the range of the horizontally integrated wind profiles; hence, we assume that the ECMWF and Loon vertical wind components are also negligible.

The *Aeolus* L2B algorithm has been continuously improved since the start of the mission, leading to several product baseline versions (ESA, 2019). One of the main achievements was the implementation of a bias-correction scheme as of baseline version 10, which is based on correlating the temperature fluctuations on the ALADIN telescope along the orbit with the mean ECMWF model

background state (Weiler *et al.*, 2021). This processor update could reduce the orbital varying wind biases in the *Aeolus* product to below $\pm 1 \text{ m}\cdot\text{s}^{-1}$ for the major portion of the data. For this purpose, the *Aeolus* wind speed bias is defined relative to the ECMWF model equivalent winds. Following this processor update, the *Aeolus* Level 1B and Level 2B products were publicly released in May 2020. The data used in this study are produced using *Aeolus* product baseline 10 and later versions (e.g., ESA, 2019; *Aeolus*-DISC, 2021).

The *Aeolus* monitoring using the ECMWF model suggests that random errors of the HLOS Rayleigh–clear wind speed have increased from about $4 \text{ m}\cdot\text{s}^{-1}$ at the start of the mission up to $7 \text{ m}\cdot\text{s}^{-1}$ at the end of 2021 (Rennie *et al.*, 2021). The increase is partially explained by the decrease in signal-to-noise ratio due to the continuous decrease in the ALADIN laser emit energy during the mission lifetime (e.g., Lux *et al.*, 2020; Reitebuch *et al.*, 2020a), and partially by a signal loss in optical emit and receive paths on the instrument (Reitebuch *et al.*, 2020b). The NWP impact of Rayleigh–clear winds is strongly affected by the noise level (Rennie *et al.*, 2021), which demonstrates that this effect is also not negligible for the scientific use of the *Aeolus* Rayleigh–clear data.

2.2 | Loon dataset

Super pressure balloons provide a unique way of measuring dynamical properties of the tropical UTLS. The balloons use inextensible, spherical envelopes with a fixed amount of gas and ascend until the altitude region where the atmospheric density matches the balloon density (Vincent and Hertzog, 2014). Once they have reached this equilibrium, they float horizontally as quasi-Lagrangian tracers with the air motion. Thus, the horizontal wind speed can be derived directly from changes in the balloon location.

Each Loon balloon was powered via a solar panel and carried a GPS position sensor, nadir-pointing radiometer, pressure and temperature sensor (Conway *et al.*, 2019). The data were sampled at 1 Hz on the balloon, but additional onboard filtering was done, hence the observations were delivered with a temporal frequency of typically 1 min using a smoothing window of 6 min (Rhodes and Candido, 2021). The observations of GPS position have uncertainties of approximately 10 m, which translates into an uncertainty of $0.23 \text{ m}\cdot\text{s}^{-1}$ in the derived meridional and zonal wind speed (Friedrich *et al.*, 2017). Further uncertainties in the Loon wind observations arise from the inertia of the large balloons, which may cause some underestimation of wind-speed differences on short time-scales (Coy *et al.*, 2019). The balloon altitude is measured in metres above mean sea level with an uncertainty of

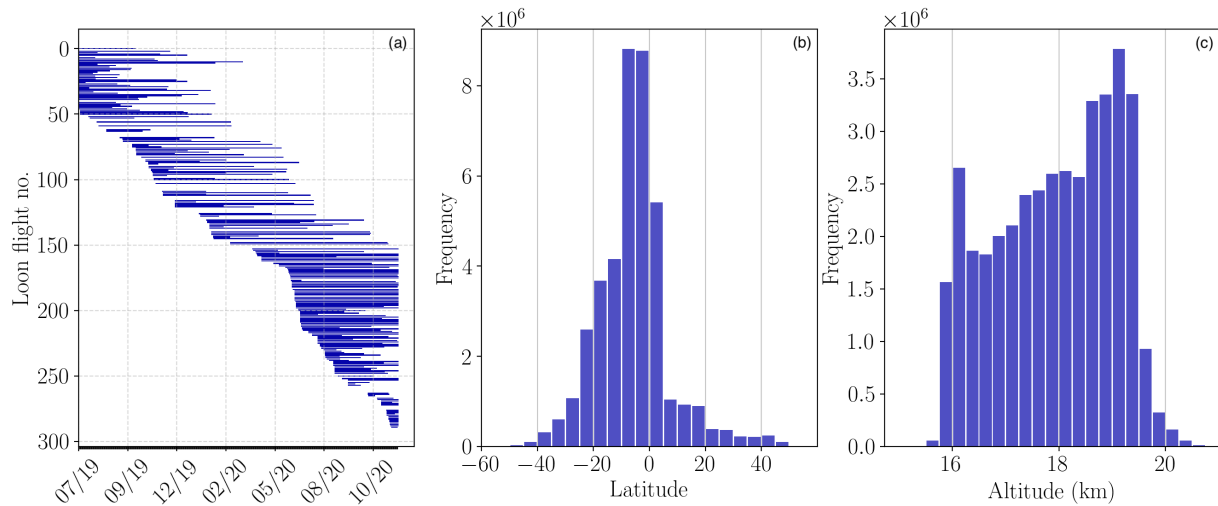


FIGURE 1 Global Loon balloon flight statistics for July 2019–December 2020, including (a) a timeline for each individual balloon flight and the distribution of Loon measurements as a function of (b) latitude and (c) altitude [Colour figure can be viewed at wileyonlinelibrary.com]

± 2.5 m. Occasionally, sudden changes of the balloon altitude occur on short time-scales, caused by manual manoeuvres in order to maintain the balloon position. When a balloon is blown away by winds from a target region, it automatically moves to another height at which it can fly back again. For making the best decisions, a neural network has been trained (Osprey, 2020). Although the Loon project stopped the operation of its balloon flights in 2021 (Spacenews, 2021), it leaves a unique long-term dataset covering the time period from 2011–2021. A comprehensive description of the Loon dataset is provided in Rhodes and Candido (2021).

In this study, we make use of the Loon super pressure balloon measurements from 229 individual flights between July 2019 and December 2020 (Rhodes and Candido, 2021). Figure 1 provides an overview of several statistics for all Loon flights considered. Most of the Loon balloons were located over the Tropics between 30°N and 30°S , and only a few balloons flew further north (40°N) or south (40°S). The integration of all 229 balloon flights results in a total flight time of 6,395 days. The flight duration of individual balloons ranged from a few days up to 227 days for the longest Loon flight. The typical altitude of the Loon balloons ranges between 16 and 20 km. This altitude region covers the tropical tropopause layer (TTL), the most important part of the tropical UTLS.

2.3 | ECMWF model winds

As complement to the comparison of *Aeolus* and Loon winds, the collocated observations are compared against the winds from the ECMWF IFS. As mentioned above, this model wind information is part of the auxiliary

meteorological (AUX_MET) data, which are used for L2B processing (De Kloe *et al.*, 2020). The AUX_MET files are produced every 12 hr (at 0600 and 1800 UTC) and contain vertical profiles of the ECMWF IFS TcO1279 L137 background forecast from 0300 and 1500 UTC along *Aeolus* predicted orbits (Rennie and Isaksen, 2020). The AUX_MET files also provide the u and v wind components as a function of geometric altitude.

From the ECMWF model, the forward-modelled wind observation equivalent (known as background) is compared with the *Aeolus* wind observation. Observation minus background (O–B) departure statistics provide valuable information on the quality of observations from a new observing system like *Aeolus* (Rennie *et al.*, 2020).

The model winds are collocated and converted to the *Aeolus* HLOS wind speed and provided in the L2B product in near-real time (NRT). Therefore, the AUX_MET provides a convenient and collocated reference wind for comparison with the *Aeolus* L2B wind product. The AUX_MET data provides up to 30-hr forecasts, but the shorter range forecasts are considered for comparison with the L2B product because they are more accurate. Further details on the AUX_MET files and the O–B statistics are provided in Rennie and Isaksen (2020).

2.4 | Comparison of the three datasets

Figure 2 shows the global distribution of collocated wind observations between Loon and *Aeolus* Rayleigh-clear winds (87-km signal averaging along the measurement track and reported at the observation centre of gravity within the respective vertical bin). For identifying these collocations, the *AeolusBalloons* tool (v1.1.1) has been

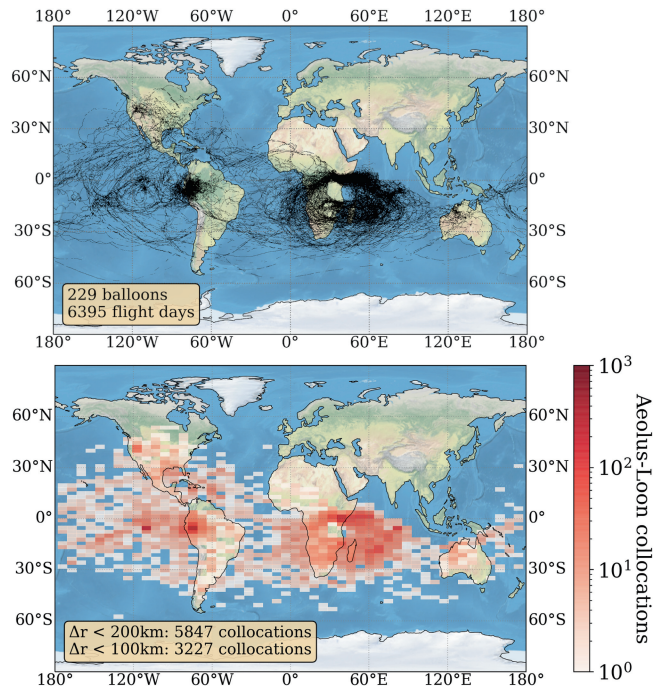


FIGURE 2 Global collocated wind observations acquired from *Aeolus* and Loon in the time period from July 2019–December 2020. The trajectories of all 229 Loon flights are shown at the top, the distribution of collocations between *Aeolus* and Loon at the bottom. The numbers of collocated observations for maximum collocation distances of 200 and 100 km are shown in the annotation box

applied, which calculates the visibility passes of the *Aeolus* swath for all balloon positions in a balloon trajectory file within a given time interval (ESA, 2020–2022). Each balloon point in a given balloon trajectory file is defined by longitude, latitude, altitude, and time. As additional input for the *Aeolus*Balloonpass tool, we set the maximum spatial and temporal difference between a certain balloon point and the *Aeolus* Rayleigh–clear wind observation (at the centre of gravity) to 200 km and 2 hr respectively. The *Aeolus*Balloonpass tool provides all Loon balloon points that meet the criteria in an output file for each *Aeolus* wind observation. The resulting balloon points are then averaged before converting u and v to the *Aeolus* HLOS wind equivalent. We consider only unique collocations for the statistical analysis, thus neither *Aeolus* observations nor Loon balloon points are used multiple times.

For assessing the impact of the collocation criteria on the number of acquired collocations, we have also applied a maximum collocation distance of 100 km (Figure 2). A total of 5,847 collocated wind observations is found for a maximum collocation distance of 200 km. The number of collocations reduces to 3,227 when applying the collocation threshold of 100 km. For determination of the optimal collocation criterion, we have estimated the variability of the horizontal wind speed by calculating the

standard deviation of collocated Loon winds within the 200-km collocation distance.

The standard deviation of Loon winds is $0.89 \text{ m}\cdot\text{s}^{-1}$ on average and ranges between 0 and $3.5 \text{ m}\cdot\text{s}^{-1}$. As described in Section 2.1, each *Aeolus* HLOS wind observation provides an estimated error statistic representative as instrument noise. The HLOS wind-error estimate for all collocated *Aeolus* Rayleigh wind measurements is $4.1 \text{ m}\cdot\text{s}^{-1}$ on average, which is significantly larger than the standard deviation of Loon winds. This result justifies the adapted collocation criteria.

We reject collocations when artificial altitude manoeuvres higher than 1,000 m occur in the Loon dataset within 2 hr. After filtering has been applied, 3,095 collocations are considered for the statistical analysis.

Figure 2 shows a high density of Loon observations over the Andes and the East African plateau. Both were target regions of the Loon project in 2019 and 2020, when the balloons were floating on constant-density surfaces.

2.5 | Statistical measures

Using the Loon wind observations or the ECMWF model winds as reference, the *Aeolus* HLOS wind-speed bias is calculated as the mean difference in the HLOS winds according to

$$\text{bias} = \frac{1}{N} \sum_{i=1}^N (\text{HLOS}_{\text{Aeolus},i} - \text{HLOS}_{\text{reference},i}), \quad (2)$$

where N is the sample size. The root-mean-square difference (RMSD) of our dataset is defined as

$$\text{RMSD} = \sqrt{\frac{1}{N-1} \sum_{i=1}^N [(\text{HLOS}_{\text{Aeolus},i} - \text{HLOS}_{\text{reference},i}) - \text{bias}]^2}, \quad (3)$$

whereas the scaled median absolute deviation (scaled MAD) is calculated using

$$\begin{aligned} \text{scaledMAD} &= 1.4826 \times \text{median} \\ &(|(\text{HLOS}_{\text{Aeolus}} - \text{HLOS}_{\text{reference}}) \\ &- \text{median}(\text{HLOS}_{\text{Aeolus}} - \text{HLOS}_{\text{reference}}))| \end{aligned} \quad (4)$$

The HLOS reference winds ($\text{HLOS}_{\text{reference},i}$) correspond to the reprojected and averaged Loon wind observations or the ECMWF model winds at the locations of *Aeolus* HLOS wind observation.

The scaled MAD is a more robust measure for the variability of wind-speed differences between *Aeolus*, Loon, and the ECMWF model compared with the RMSD. The scaled MAD has a further advantage that it is less sensitive to single outliers. In the case in which that the wind differences used to evaluate the RMSD in Equation (3) are Gaussian-distributed, the scaled MAD is equivalent to the RMSD (Ruppert and Matteson, 2011).

2.6 | Estimation of representativeness errors

The different measurement geometries as well as the spatial and temporal displacement between the balloon and the *Aeolus* observations contribute to the representativeness errors. For the ECMWF model, the representativeness error can be calculated by comparing the model equivalents of the HLOS winds at the *Aeolus* observation centre of gravity and the average HLOS wind along the *Aeolus* observation scale of 87 km. This is built on the fact that *Aeolus* observations are considered as point winds in the assimilation system, whereas the actual *Aeolus* HLOS wind observation represents the average of 87 km. Because we compare *Aeolus* winds against much higher resolved balloon observations, we assume that they can be used to estimate the *Aeolus* representativeness errors.

While *Aeolus* provides profiles of the single HLOS wind component, the Loon balloons deliver the full zonal and meridional wind components (see Section 2.4). Each *Aeolus* Rayleigh-clear wind observation has a horizontal

resolution of typically 87 km and a vertical resolution between 1 and 2 km at the altitude of the balloons. The Loon wind observations are calculated using a 6-min smoothing window. This results in a horizontal resolution of a few hundred metres up to a few kilometres depending on the wind speed. Thus, Loon winds provide highly resolved information about the variability of the horizontal wind field, while *Aeolus* wind profiles only represent the average wind over 87 km along the instrument measurement track. Because the HLOS wind speed is measured perpendicular to the flight track, this average contains parts of the zonal wind variability along the flight track only.

We estimate the representativeness error of *Aeolus* HLOS winds in the UTLS by calculating the standard deviation of Loon winds for trajectory segments of 200 km centred around the *Aeolus* overpass location. The results have been averaged for different altitude regions between 16 and 20 km, as shown in Figure 3a. The HLOS representativeness error is found to be between 0.6 and 1.1 $\text{m}\cdot\text{s}^{-1}$. The values are smallest around 16 km and increase with altitude until 18 km, while between 18 and 20 km the values are constantly around 1 $\text{m}\cdot\text{s}^{-1}$. Despite the relatively large area of 200 km, the observed horizontal variability of the wind speed seems rather small. These results demonstrate that the horizontal integration length is sufficient for *Aeolus* Rayleigh-clear winds to represent the zonal wind speed in the tropical UTLS well.

In contrast, the *Aeolus* wind profiles are more poorly resolved in the vertical dimension in the UTLS, where the range-bin width is between 0.75 and 1.25 km for the

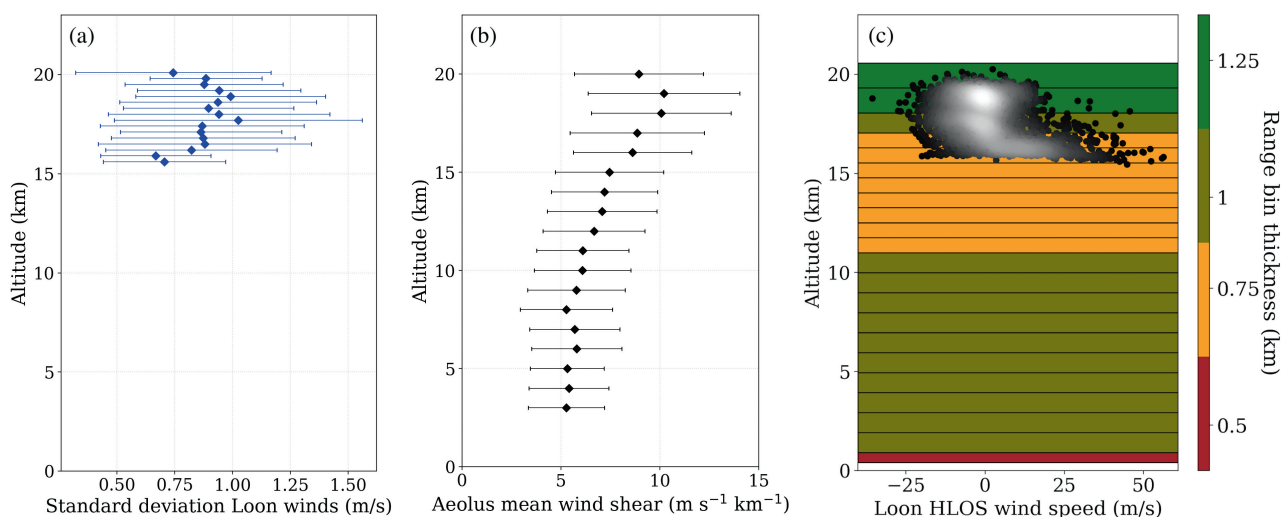


FIGURE 3 (a) Representativeness error of *Aeolus* Rayleigh-clear winds, estimated from the standard deviation of Loon winds considered for the comparison with *Aeolus* as a function of altitude. (b) Mean *Aeolus* HLOS wind shear for all collocated profiles. (c) Overview of mean *Aeolus* Rayleigh-clear wind range bin width including the distribution of Loon observations. The error bars indicate the 75% confidence interval for each altitude level

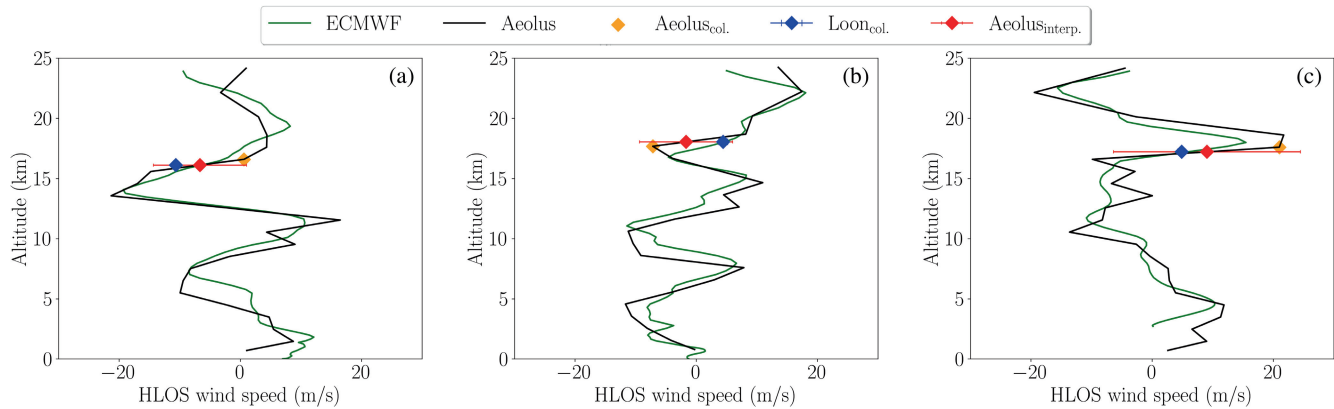


FIGURE 4 Three example *Aeolus* Rayleigh-clear HLOS wind profiles (black solid line) including the collocated Loon wind observation (blue) and the ECMWF model winds (green lines) at the following locations: (a) lon=111°W, lat=1°S; (b) lon=80°W, lat=6°S; (c) lon=80°W, lat=7°S. The yellow marker indicates the *Aeolus* wind speed of the vertical range bin closest to the Loon altitude, while the red marker shows the HLOS wind observations interpolated between the range bins below and above the Loon altitude. The horizontal error bars represent the RMSD of wind-speed differences

time period analysed. In the tropical UTLS region, the wind speed can significantly vary with altitude, reaching wind-shear values up to $20 \text{ m}\cdot\text{s}^{-1}\cdot\text{km}^{-1}$ (e.g., Houchi *et al.*, 2010; Rennie and Isaksen, 2020). Figure 3b shows the *Aeolus* HLOS mean wind shear for all profiles analysed between 3 and 20 km. The mean wind shear is found to be around $5 \text{ m}\cdot\text{s}^{-1}\cdot\text{km}^{-1}$ in the lower troposphere, increases in the free troposphere, and reaches mean values of $8\text{--}10 \text{ m}\cdot\text{s}^{-1}\cdot\text{km}^{-1}$ between 17 and 20 km.

Figure 3c provides an overview of the typical *Aeolus* range-bin width in the Tropics, including an overlay of the collocated mean Loon wind observations. The Tropical *Aeolus* range bin setting covers the whole troposphere from the ground up to the lower stratosphere, with one 500-m bin at the ground, 1-km bins up to 11-km, and 750-m bins in the upper troposphere. The three range bins above are getting slightly thicker again. This setting covers large parts of the globe from 30°S to 30°N, the region where most of the Loon observations are found. All Loon winds are located within five *Aeolus* range bins with varying vertical resolution between 0.75 and 1.25 km. A clear lower-boundary flight altitude at around 16 km can be seen. No significant range-bin dependent wind bias was found in our study.

Figure 4 shows three example Rayleigh-clear HLOS wind profiles including the collocated Loon observation and ECMWF model reference wind. One profile is over the South Pacific near the Equator (Figure 4a), the other two profiles are over the Andes region.

Both Loon and ECMWF wind components have been converted to the HLOS wind speed of *Aeolus*. The ECMWF wind profile is shown in its original vertical resolution with 137 vertical layers, but cut at the upper bound of the *Aeolus* profiles. Despite the coarser vertical resolution, *Aeolus*

is also able to capture the strong wind speed peaks in situations with strong wind shear. Another challenge becomes visible here. Only a small change in the altitude of the Loon balloons can cause a significant difference in wind speed, particularly in situations with strong wind shear. If the balloon target altitude lies between two *Aeolus* range bins, both *Aeolus* HLOS results might deviate from the wind speed observed by Loon. A simple average of two *Aeolus* range bins does not solve this problem. Therefore, we have linearly interpolated the *Aeolus* HLOS wind results between the *Aeolus* range bins below and above the Loon observation in order to approximate the *Aeolus* measurement at the altitude of the balloon better. Applying this method reduces the wind difference between *Aeolus* and Loon in the majority of cases. This finding highlights the need for a more realistic HLOS wind observation operator for assimilating *Aeolus* winds in the ECMWF model, instead of considering them as point winds (located at the centre of gravity of the Rayleigh wind observations within a vertical height bin and within the 87-km along-track averaging), as is currently done in the ECMWF forward model. This also underlines the need for finer vertical sampling in a potential *Aeolus* follow-on mission. This is currently being studied by ESA and EUMETSAT in the frame of the Doppler wind lidar/*Aeolus*-2 activities (Heliere *et al.*, 2021).

3 | RESULTS

3.1 | *Aeolus* versus Loon

Figure 5 shows the comparison of all *Aeolus* L2B Rayleigh-clear wind products against collocated wind

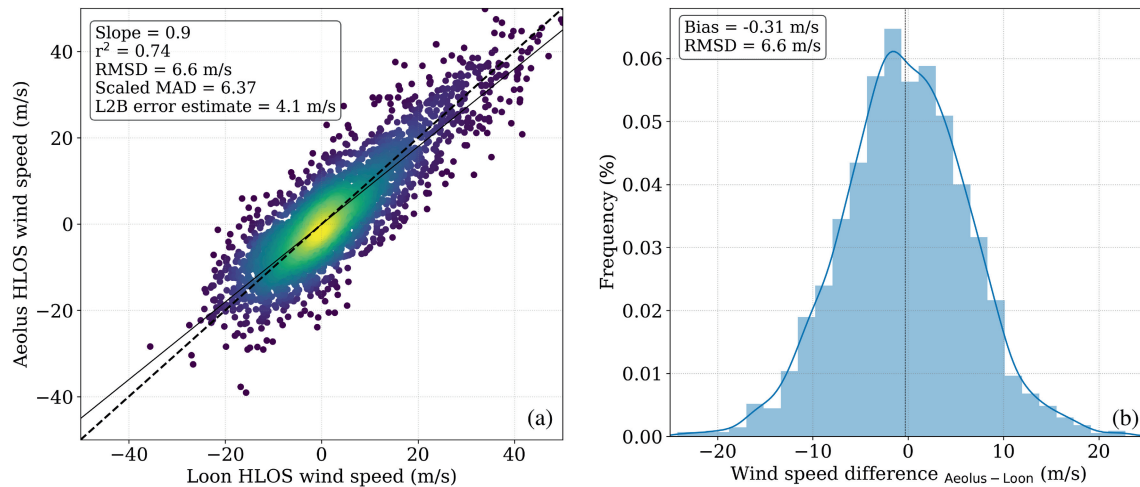


FIGURE 5 (a) *Aeolus* HLOS Rayleigh-clear winds versus collocated Loon winds, projected and converted to the *Aeolus* HLOS winds. The corresponding least-squares fit line is indicated by the black solid line, the dashed line shows the $x = y$ line. (b) Histogram of the HLOS wind-speed difference between *Aeolus* and Loon for the same dataset as in (a). The slope, correlation coefficient, RMSD, scaled MAD L2B instrument-error estimate, and HLOS wind bias are shown in the annotation boxes

information from the Loon balloon data. In general, the *Aeolus* L2B Rayleigh-clear winds are found to be in good agreement with collocated Loon winds, with a systematic error of $-0.31 \text{ m}\cdot\text{s}^{-1}$ on average for the full time period. The RMSD of wind-speed differences provided by the linear fit is $6.6 \text{ m}\cdot\text{s}^{-1}$ and the average error estimate of the L2B Rayleigh-clear wind product is $4.1 \text{ m}\cdot\text{s}^{-1}$. As explained in Section 2.5, the scaled MAD is considered as the best approximation of the random error of *Aeolus* winds, instead of the RMSD of wind-speed differences. It is found to be $6.37 \text{ m}\cdot\text{s}^{-1}$ using Loon winds as reference (Figure 5). The low wind bias is in agreement with the expectations of the bias-corrected L2B wind products. The scaled MAD, which is considered as the random error of the wind-speed differences between *Aeolus* and Loon, is significantly larger than the Rayleigh-clear wind-error estimate. The Rayleigh wind-error estimate, however, only accounts for a subset of instrument noise and thus is expected to underestimate the real wind random error. This is partly why, when using the error estimate from the L2B product in data assimilation experiments, it is scaled by a factor of 1.4 (Rennie and Isaksen, 2020). This specific scaling factor chosen is unique to the ECMWF, while other NWP centres use different methods for defining the assigned observation error in their data assimilation systems. In the following, the scaled MAD calculated by means of collocated Loon observations is compared with other studies validating *Aeolus* winds.

Since the *Aeolus* launch in 2018, the *Aeolus* DISC and external validation teams have performed comprehensive validation studies to assess the quality of the *Aeolus* wind and aerosol/cloud products. The following

review of results is limited to wind validation studies. Baars *et al.* (2020) have compared *Aeolus* winds with collocated winds measured from radiosondes, which have been launched from the research vessel *Polarstern* during a cruise in November and December 2019. Their results yield a scaled MAD of $4.84 \text{ m}\cdot\text{s}^{-1}$ for Rayleigh-clear winds. Two important aircraft campaigns, called Wind Validation (WindVal) III (Lux *et al.*, 2020) and AVATAR-E (Witschas *et al.*, 2020), were conducted in November 2018 and May 2019. *Aeolus* Rayleigh-clear winds have been validated against collocated HLOS winds measured from the ALADIN Airborne Demonstrator (A2D). In conclusion, the scaled MAD $3.6 \text{ m}\cdot\text{s}^{-1}$ for WindVal III and $4.4 \text{ m}\cdot\text{s}^{-1}$ for AVATAR-E. Martin *et al.* (2021) performed a validation study of *Aeolus* Rayleigh-clear and Mie-cloudy winds against radiosonde observations and model data over the Northern Hemisphere for a long time period from September 2018–December 2019. The comparison between *Aeolus* Rayleigh-clear winds and radiosonde observations resulted in a scaled MAD of $5.07 \text{ m}\cdot\text{s}^{-1}$ for ascending and $4.95 \text{ m}\cdot\text{s}^{-1}$ for descending orbits, respectively. Belova *et al.* (2021) used ground-based radars in Antarctica and in Northern Sweden for validation of *Aeolus* winds from July–December 2019. The random error for *Aeolus* Rayleigh-clear winds varies between 5.4 and $7 \text{ m}\cdot\text{s}^{-1}$, with higher random errors in summer compared with winter. The latter results are due to the high-latitude location of the two ground-based sites, and hence the higher solar background contribution in the *Aeolus* observations during polar summer.

When contrasting these findings with the result of the present study, it is noticed that the scaled MAD of

$6.37 \text{ m}\cdot\text{s}^{-1}$ is at the upper range of other validation studies. It is important to mention here that most studies focus on lower tropospheric levels below the UTLS, where the *Aeolus* winds are expected to have higher precision when the vertical wind shear is smaller. Furthermore, the vertical wind shear peaks in the tropical UTLS due to the occurrence of planetary and gravity waves, which provide an additional source for an increase in the noise of *Aeolus* winds. The majority of experiments or campaigns are from earlier time periods in the mission. It is known that the random errors of the *Aeolus* Rayleigh wind product has increased with time, as is described in Section 2.1. Whether this trend can be confirmed by the comparison between *Aeolus* and Loon is investigated in Section 3.3.

3.2 | *Aeolus* and Loon versus ECMWF model

One important element for the assessment of the *Aeolus* wind-product quality is the operational monitoring of *Aeolus* winds using the NWP model from ECMWF (Rennie *et al.*, 2021). O–B departure statistics have shown random errors for the *Aeolus* Rayleigh-c wind product ranging from $4\text{--}7 \text{ m}\cdot\text{s}^{-1}$. These results are representative for the whole globe and for all vertical range-bin levels of *Aeolus*. The cause for this large range of random errors is explained in Section 2.1.

In the analysis performed here, the bias statistics using the ECMWF model winds were acquired only for the locations of the collocated *Aeolus* and Loon observations. Hence, these statistics mainly represent the systematic and random errors of the *Aeolus* and Loon wind observations in the tropical UTLS.

Figure 6a,b shows the differences between Rayleigh-clear winds observed from *Aeolus* and the HLOS forecast winds from the ECMWF model at the *Aeolus* location, as provided in the L2B product (see Section 2.3). Thus, collocation or conversion to the HLOS wind speed is not required. This is not as straightforward for the comparison of Loon data with the ECMWF model (Figure 6c,d). In general, the ECMWF model provides the horizontal wind components u and v with a higher spatial resolution compared with the *Aeolus* observation scale of 86 km for Rayleigh winds. However, because this study focuses on the comparison between *Aeolus* and Loon winds, we only consider the ECMWF reference wind already converted to the *Aeolus* HLOS wind speed for the comparison with Loon. The difference between *Aeolus* and ECMWF depicts a HLOS wind bias of $0.18 \text{ m}\cdot\text{s}^{-1}$ and a random error of $5.96 \text{ m}\cdot\text{s}^{-1}$, which is in the same range as shown by NWP monitoring results (Rennie *et al.*, 2021). In comparison with the ECMWF forecast winds, the Loon balloon

wind bias and random error are 0.49 and $4.03 \text{ m}\cdot\text{s}^{-1}$ respectively.

Hertzog *et al.* (2004) compared winds from super pressure balloons against the ECMWF in the Northern Hemisphere and found a bias of $0.3 \text{ m}\cdot\text{s}^{-1}$ and random errors in the range $2.3\text{--}2.7 \text{ m}\cdot\text{s}^{-1}$. Friedrich *et al.* (2017) compared Loon winds, measured in 2014, with different reanalysis data and found biases for the zonal wind speed of less than $0.37 \text{ m}\cdot\text{s}^{-1}$ and random errors ranging between 2.5 and $3.5 \text{ m}\cdot\text{s}^{-1}$.

Our results on the systematic wind error are consistent with the findings of both of these balloon studies, but the random error of $4.03 \text{ m}\cdot\text{s}^{-1}$ is significantly larger. Most likely, this is due to our applied collocation criteria and the averaging of ECMWF model winds to the coarser *Aeolus* observation scale.

Because it can be assumed that wind observations from super pressure balloons have a very high precision (see Section 2.2), the random errors between Loon and the ECMWF model are likely due to random errors, biases, or other uncertainties in the ECMWF forecast.

3.3 | Time series of wind biases and random errors

Figure 7 shows the time series of systematic and random errors of *Aeolus* Rayleigh-clear winds for the time period from July 2019–December 2020 in the tropical UTLS relative to Loon balloon observations and ECMWF model winds. It must be stated that, although the ECMWF model does not represent the truth, it provides a valuable reference to the *Aeolus* observations in the UTLS additional to the Loon balloon observations. Therefore we aim to present the *Aeolus* HLOS wind-speed differences relative to both reference datasets in one figure.

The time-series curves are generated by calculating the daily mean values before applying a seven-day rolling median filter. This is done to facilitate comparability with the operational O–B departure statistics, because they are calculated for a larger sample size.

The time series of wind-speed biases between *Aeolus*–Loon and *Aeolus*–ECMWF exhibits values varying between -2 and $2 \text{ m}\cdot\text{s}^{-1}$, while the *Aeolus*–ECMWF biases are slightly smaller. No significant trend can be derived for the wind bias. In contrast, the *Aeolus*–Loon random errors range from around $5 \text{ m}\cdot\text{s}^{-1}$ in July 2019 to $7 \text{ m}\cdot\text{s}^{-1}$ in December 2020. This increase in random error is in agreement with findings by Rennie *et al.* (2021), who found an increase of $1 \text{ m}\cdot\text{s}^{-1}$ when comparing August 2019 and August 2020.

In order to exclude contributions from the balloon wind bias and the horizontal wind variability, we subtract

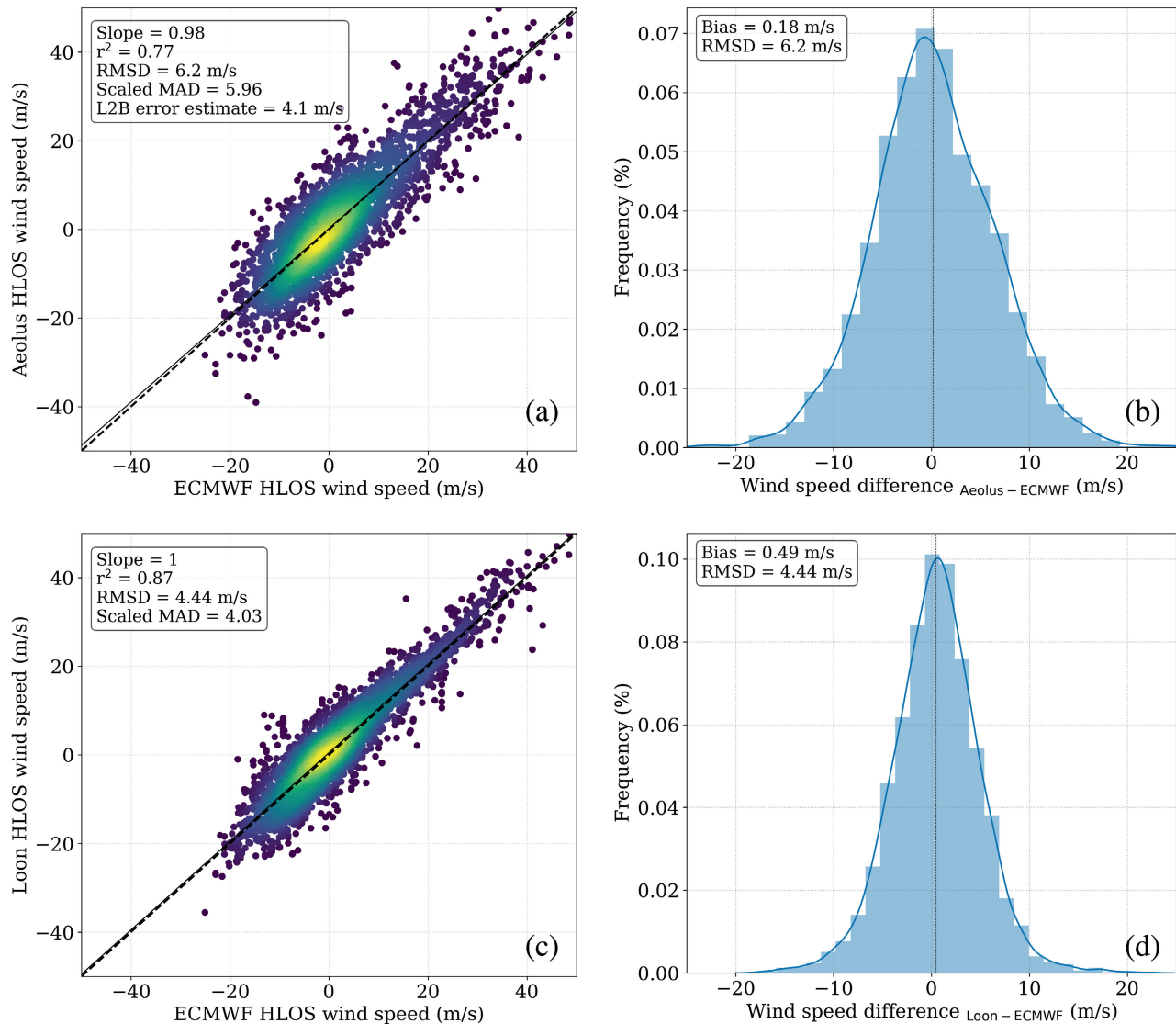


FIGURE 6 Comparison of HLOS Rayleigh-clear winds between (a,b) *Aeolus* and ECMWF forecasts and between (c,d) Loon observations and ECMWF forecasts. The Loon HLOS winds are not at their original resolution, but averaged and converted to the *Aeolus* HLOS Rayleigh-clear observation scale. Description of the markers, fit lines, and annotation boxes is the same as in Figure 5

the Rayleigh wind representativeness error of 0.8 m s^{-1} and the assumed balloon bias of 0.23 m s^{-1} from the random error of the *Aeolus*–Loon wind-speed differences. After this correction, the time series of the *Aeolus*–Loon random error agrees very well with the time series from O–B statistics (blue and black solid lines in Figure 7).

The black curves show results from the operational *Aeolus* HLOS Rayleigh-clear wind-product quality monitoring done at ECMWF. These results have been added to expand the intercomparison between *Aeolus* and ECMWF from the collocations between *Aeolus* and Loon balloons to the whole tropical UTLS region. With this approach, we can exclude the impact of local or temporal effects, because the Loon data are not distributed homogeneously over

the Tropics. Thus (O–B) departure statistics have been calculated from 30°N – 30°S and for pressure levels from 60–120 hPa, the altitude region where the balloons were present.

Before May 2020, the systematic HLOS wind error via O–B deviates from the green dotted lines. This is due to the major bias correction scheme, which has been introduced in May 2020 (e.g. Rennie *et al.*, 2021; Weiler *et al.*, 2021). With the activation of this bias correction in the L2B wind processor, the global systematic error was reduced significantly to values below $\pm 1 \text{ m s}^{-1}$ for the major portion of the data (grey shaded area in Figure 7). As described in Section 2.1, we have used the latest reprocessed dataset for the full period, with global wind biases below $\pm 1 \text{ m s}^{-1}$, while the O–B statistics are based on

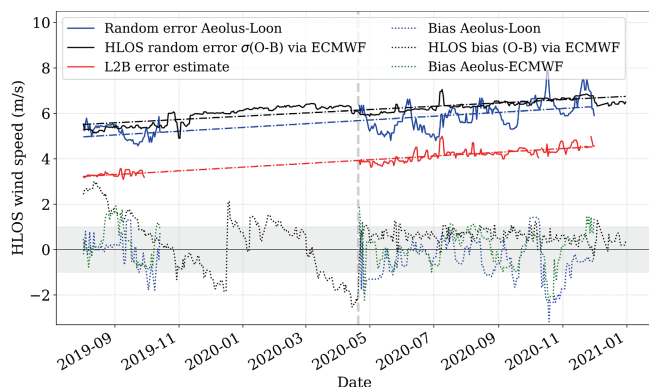


FIGURE 7 Time series of the systematic wind-speed differences between *Aeolus* and Loon (blue dotted), *Aeolus* and ECMWF (green dotted), and *Aeolus* and ECMWF calculated from operational O–B statistics (black dotted). The black solid line indicates the random error of O–B wind departures, calculated between 30°N and 30°S and for pressure levels from 60 to 120 hPa. The blue solid line shows the scaled MAD of wind differences between *Aeolus* and Loon, corrected by the Loon observation error and the horizontal representativeness error. All lines are produced by calculating daily mean values first and applying a seven-day rolling median filter. The red line shows the L2B product error estimate for Rayleigh–clear winds. The grey dashed line marks the date when the bias-correction scheme was introduced with baseline 10. The grey shaded area shows the boundaries for the wind bias between $\pm 1 \text{ m}\cdot\text{s}^{-1}$. The gap between October and December 2019 marks a period when no Loon data are available

the operational NRT dataset, which also includes periods before that bias correction was introduced. Rennie *et al.* (2021) reported that the global average bias of *Aeolus* Rayleigh winds is around $0 \text{ m}\cdot\text{s}^{-1}$ after the bias correction in May 2020. When concentrating solely on the tropical UTLS, however, the O–B results indicate a bias of $1 \text{ m}\cdot\text{s}^{-1}$, while the wind differences between *Aeolus* and Loon vary around $0 \text{ m}\cdot\text{s}^{-1}$ (Figure 7). When having a closer look at the bias between *Aeolus*–Loon and *Aeolus*–ECMWF, we also notice a positive offset of *Aeolus*–ECMWF compared with *Aeolus*–Loon, with values between 0.5 and $1 \text{ m}\cdot\text{s}^{-1}$ (Figure 7). This finding indicates that the ECMWF model forecast underestimates the zonal wind in the tropical UTLS.

4 | DISCUSSION

In comparison with wind measurements from the Loon super pressure balloon network, the systematic and random errors of *Aeolus* HLOS winds are found to be -0.31 and $6.37 \text{ m}\cdot\text{s}^{-1}$ in the tropical UTLS. ESA’s pre-launch mission requirements aimed for a random error of $3 \text{ m}\cdot\text{s}^{-1}$ in that altitude range (Ingmann and Straume, 2016).

Furthermore, the target for the *Aeolus* wind bias was set to $0.7 \text{ m}\cdot\text{s}^{-1}$ over all vertical range-bin levels. While the bias, as elaborated in this study for the tropical UTLS, is within the mission requirements, the random error significantly exceeds them. The low wind bias is the main achievement of the bias-correction scheme using the ALADIN telescope temperature fluctuations (for details see Section 2.1). The main reason for not reaching the targeted random error for *Aeolus* Rayleigh winds is the lower than expected laser output energy (between 60 and 70 mJ as opposed to 80 mJ as intended prior to launch) and the higher than expected signal loss in the optical emit and receive path of the instrument. A comprehensive view of the causes for this loss are given in Lux *et al.* (2020) and Reitebuch *et al.* (2020b).

The results show that the HLOS wind-error estimate underestimates the random error of the *Aeolus* wind speed in the tropical UTLS. We found random errors that are about $2 \text{ m}\cdot\text{s}^{-1}$ higher than the error estimate of the L2B product. It has been explained earlier in this study that the L2B wind-error estimate is an error statistic taking into account the instrument noise and thus cannot be expected to represent the full random error of the *Aeolus* winds. However, as can be seen from Figure 7, the reported random error is still quite accurate and can be used for quality control using a constant multiplier.

Looking into *Aeolus* wind profiles, we found mean wind-shear values of $10 \text{ m}\cdot\text{s}^{-1}\cdot\text{km}^{-1}$, while the maximum values might be much higher in situations with strong wind shear. Houchi *et al.* (2010) show that the vertical wind shear is underestimated in the ECMWF model compared with radiosonde observations. By applying vertical averaging of the radiosonde data at different vertical resolutions, it is demonstrated that the ECMWF model has an effective vertical resolution of 1.7 km in the free troposphere (Houchi *et al.*, 2010). In comparison with the ECMWF, *Aeolus* measurements offer a slightly better vertical resolution in the UTLS. Banyard *et al.* (2021) demonstrated that *Aeolus* is able to provide unique information on gravity-wave structures and propagation in the UTLS region. This information can be used to quantify model errors and to constrain gravity wave parameterizations in models better. A large proportion of Loon measurements are found over the Andes region. The collocated *Aeolus* wind profiles indicate gravity-wave structures in that region, as shown in Figure 4b,c.

Wergen (2011) demonstrated that the *Aeolus* observation error used in data assimilation experiments underestimates the real random error of Rayleigh winds by $1\text{--}2 \text{ m}\cdot\text{s}^{-1}$ in situations with high turbulence. The tropical UTLS and areas characterized by orographically induced gravity waves are typical areas for such situations and thus it is expected that the random error of *Aeolus* winds in the UTLS will be higher compared

with the global average. An improvement of the *Aeolus* vertical resolution of 750 m or better could potentially lead to a better representation of the dynamics in the UTLS, despite the likely resulting increased random errors due to the lower atmospheric and instrumental signal with the current setup. This motivates the user requirement for a higher vertical resolution for *Aeolus*-2 (Heliere *et al.*, 2021).

The time series of the *Aeolus* Rayleigh-clear wind bias indicates that the ECMWF model forecast underestimates the wind speed in the tropical UTLS by about $1 \text{ m}\cdot\text{s}^{-1}$. The same feature was visible in the O-B departure statistics for the whole tropical UTLS between 30°N and 30°S , which confirms that this is not an artefact. It could be also demonstrated that it is not due to a systematic error of *Aeolus* Rayleigh-clear winds, because, in comparison with Loon winds, they are found to be unbiased on average.

Although the full dataset from 229 balloon flights covers large areas of the Tropics around the globe, it might not be representative for the highest observed wind velocities. This is not surprising when considering the main purpose of Loon balloons, which is preferably to remain locally constant for a long time period. Thus, the balloons mainly fly in low wind regimes, unless they are travelling to their target region. We found maximum values of approximately $40 \text{ m}\cdot\text{s}^{-1}$ (Figure 5). It would be interesting to compare our results with those from the Stratéole-2 campaign in the future (Hertzog and Plougonven, 2021), because the balloons fly in the same altitude regime but without performing manoeuvres. In total, Stratéole-2 will release 50 super pressure balloons in three campaigns between 2019 and 2024 (Corcos *et al.*, 2021). This will allow a continuation of the *Aeolus* validation activities in the tropical UTLS after the shutdown of the Loon project.

5 | CONCLUSIONS

Wind observations from the novel *Aeolus* satellite mission address a significant gap in the global observing system, especially in the upper troposphere and lower stratosphere (UTLS). This study has validated the *Aeolus* wind product against collocated winds from the Loon super pressure balloon network, which flew in altitude regions between 16 and 20 km, providing the zonal and meridional wind components from the GPS sensors on board the balloons.

Data from 229 individual balloon flights in the tropical UTLS were analysed, applying a collocation criterion of 2 hr and 200 km. The comparison of *Aeolus* and Loon data shows systematic and random errors of -0.31

and $6.37 \text{ m}\cdot\text{s}^{-1}$, respectively, for the *Aeolus* Rayleigh-clear winds. Time series analysis showed that the random errors have increased from around $5 \text{ m}\cdot\text{s}^{-1}$ in mid 2019 up to $7 \text{ m}\cdot\text{s}^{-1}$ at the end of 2020. This finding is in agreement with other *Aeolus* long-term validation studies such as Martin *et al.* (2021), Reitebuch *et al.* (2020b), and Reitebuch *et al.* (2020a), as well as NWP monitoring results using the ECMWF model (Rennie *et al.*, 2021).

Due to its measurement principle, *Aeolus* mainly provides close to zonal wind information during the major part of the orbit. Since super pressure balloons provide temporally highly resolved information about the zonal wind velocity, we used the Loon dataset to characterize the horizontal representativeness error of *Aeolus* winds in the UTLS, which was found to be $0.6\text{--}1.1 \text{ m}\cdot\text{s}^{-1}$ depending on the altitude. In contrast, the *Aeolus* wind profiles are more poorly resolved in the vertical dimension, where the range-bin thickness is typically between 0.75 and 1.25 km. This can lead to large uncertainties in situations when the wind shear is high. Nevertheless, *Aeolus* is also able to provide the correct wind speed in such situations, which has been proven by means of Loon observations and wind forecasts from the ECMWF model. While *Aeolus* winds are currently considered as point winds by the ECMWF data assimilation system, the results of the present study highlight the need for a more realistic HLOS wind observation operator for assimilating *Aeolus* winds.

The *Aeolus* and Loon datasets were also compared against ECMWF model forecasts. The random errors of Loon winds are much smaller compared with those found for *Aeolus* winds. This result supports the suggestion that the random error of *Aeolus* winds is a dominating contribution in the comparison of *Aeolus* and ECMWF winds. The Loon wind dataset also confirms that the removal of wind biases in the *Aeolus* wind product has been done successfully. The comparison of *Aeolus* and Loon datasets against ECMWF model forecasts also suggests that the model systematically underestimates the HLOS winds in the tropical UTLS by about $1 \text{ m}\cdot\text{s}^{-1}$. While the ECMWF model winds are assumed to be almost unbiased in the global average, the results in this study suggest that this assumption is invalid in the tropical UTLS region.

Because super pressure balloons provide accurate information about the horizontal wind speed in the UTLS, they can also be considered as a unique reference dataset for the validation of future Doppler wind lidar missions.

The results elaborated in this study furthermore lead to the recommendation to increase the vertical resolution of measured wind profiles to at least 750 m in the tropical UTLS in order to characterize gravity-wave structures better. The minimum possible vertical resolution for Doppler

wind lidar missions is limited by the signal-to-noise ratio in the cloud-free atmosphere, especially in the UTLS, where few molecules are available for scattering of the lidar signal. As shown in this study, observations from the Loon balloons indicate a relatively low variability of the wind speed in the horizontal dimension, while profiles from *Aeolus* and the ECMWF model show a much larger variability in the vertical dimension. These findings suggest increasing the horizontal integration length of the lidar return signal while increasing the vertical resolution of the profiles in order to maintain the signal-to-noise ratio and maximize the information content for assimilation of *Aeolus* winds in NWP models. Therefore, this study also supports the request by the *Aeolus* scientific community for a finer vertical sampling for the proposed *Aeolus* follow-on mission Doppler wind lidar/*Aeolus-2*.

AUTHOR CONTRIBUTIONS

Sebastian Bley: conceptualization; data curation; investigation; methodology; validation; visualization; writing – original draft. **Michael Rennie:** data curation; investigation; visualization; writing – review and editing. **Nedjeljka Žagar:** investigation; writing – review and editing. **Montserrat Pinol Sole:** data curation; methodology; software. **Anne Grete Straume:** investigation; project administration; supervision; writing – review and editing. **James Antifaev:** data curation; resources. **Salvatore Candido:** data curation; resources. **Robert Carver:** data curation; resources. **Thorsten Fehr:** conceptualization; funding acquisition; project administration. **Jonas von Bismarck:** funding acquisition; investigation; project administration; supervision. **Anja Hünerbein:** conceptualization; supervision; writing – review and editing. **Hartwig Deneke:** supervision; writing – review and editing.

ACKNOWLEDGEMENTS

This research is funded by the European Space Agency (ESA) in the framework of the activities of the *Aeolus* DISC (Data Innovation and Science Cluster) consortium. The processor development, improvement, and product reprocessing preparation are performed by the *Aeolus* DISC (Data, Innovation and Science Cluster), which involves DLR, DoRIT, ECMWF, KNMI, CNRS, S&T, ABB, Serco and TROPOS, in close cooperation with the *Aeolus* PDGS (Payload Data Ground Segment). Open Access funding enabled and organized by Projekt DEAL.

CONFLICT OF INTEREST

The authors declare that they have no conflict of interest.

ORCID

Sebastian Bley  <https://orcid.org/0000-0003-1119-7067>

REFERENCES

- Aeolus*-DISC (2021) *Summary of quality of Aeolus data products from 2nd reprocessing campaign covering June 2019 to October 2020*. ESA. Technical report. Available at: <https://earth.esa.int/eogateway/documents/20142/0/Aeolus-Summary-Reprocessing-2-DISC.pdf/1ba69574-4b71-f185-f5e6-6ade0a2af7b6>.
- Baars, H., Herzog, A., Heese, B., Ohneiser, K., Hanbuch, K., Hofer, J., Yin, Z., Engelmann, R. and Wandinger, U. (2020) Validation of *Aeolus* wind products above the Atlantic Ocean. *Atmospheric Measurement Techniques*, 13, 6007–6024. <https://doi.org/10.5194/amt-13-6007-2020>.
- Baker, W.E., Atlas, R., Cardinali, C., Clement, A., Emmitt, G.D., Gentry, B.M., Hardesty, R.M., Källén, E., Kavaya, M.J., Langland, R., Ma, Z., Masutani, M., McCarty, W., Pierce, R.B., Pu, Z., Riishøjgaard, L.P., Ryan, J., Tucker, S., Weissmann, M. and Yoe, J.G. (2014) Lidar-measured wind profiles: the missing link in the global observing system. *Bulletin of the American Meteorological Society*, 95, 543–564.
- Banyard, T.P., Wright, C.J., Hindley, N.P., Halloran, G., Krisch, I., Kailer, B. and Hoffmann, L. (2021) Atmospheric gravity waves in *Aeolus* wind lidar observations. *Geophysical Research Letters*, 48, e2021GL092756. <https://doi.org/10.1029/2021GL092756>.
- Belova, E., Kirkwood, S., Voelger, P., Chatterjee, S., Satheesan, K., Hagelin, S., Lindskog, M. and Körnich, H. (2021) Validation of *Aeolus* winds using ground-based radars in Antarctica and in northern Sweden. *Atmospheric Measurement Techniques Discussions*, 14, 5415–5428. <https://doi.org/10.5194/amt-14-5415-2021>.
- Borde, R. and Arriaga, A. (2004) Atmospheric motion vectors height assignment techniques with meteosat-8. In: *Proceedings of the 7th International Winds Workshop*, CiteseerX, pp. 139–146. Available at: <https://citeseerx.ist.psu.edu/viewdoc/download?doi=10.1.1.483.2279&rep=rep1&type=pdf>.
- Conway, J., Bodeker, G., Waugh, D., Murphy, D., Cameron, C. and Lewis, J. (2019) Using project loon superpressure balloon observations to investigate the inertial peak in the intrinsic wind spectrum in the midlatitude stratosphere. *Journal of Geophysical Research: Atmospheres*, 124, 8594–8604. <https://doi.org/10.1029/2018JD030195>.
- Corcos, M., Hertzog, A., Plougonven, R. and Podglajen, A. (2021) Observation of gravity waves at the tropical tropopause using superpressure balloons. *Journal of Geophysical Research: Atmospheres*, 126, e2021JD035165. <https://doi.org/10.1029/2021JD035165>.
- Coy, L., Schoeberl, M.R., Pawson, S., Candido, S. and Carver, R.W. (2019) Global assimilation of loon stratospheric balloon observations. *Journal of Geophysical Research: Atmospheres*, 124, 3005–3019. <https://doi.org/10.1029/2018JD029673>.
- Dabas, A., Denneulin, M., Flamant, P., Loth, C., Garnier, A. and Dolfi-Bouteyre, A. (2008) Correcting winds measured with a rayleigh doppler lidar from pressure and temperature effects. *Tellus A: Dynamic Meteorology and Oceanography*, 60, 206–215. <https://doi.org/10.1111/j.1600-0870.2007.00284.x>.

- De Kloe, J., Stoffelen, A., Tan, D., Andersson, E., Rennie, M., Dabas, A., Poli, P. and Huber, D. (2020) *ADM-Aeolus Level-2B/2C processor input/output data definitions interface control document*. Technical report 3.40, AED-SD-ECMWF-L2B-037. Available at: <https://earth.esa.int/eogateway/documents/20142/37627/Aeolus-L2B-2C-Input-Output-DD-ICD.pdf>.
- ESA (1999) *The four candidate earth explorer core missions: atmospheric dynamics mission*. ESA. SP-1233, p. 145. Available at: <https://earth.esa.int/eogateway/documents/20142/37627/The%20four%20Candidate%20Earth%20Explorer%20Core%20Missions%20-%20Atmospheric%20Dynamics%20Mission?text=worldview-3>.
- ESA (2019) *Aeolus product baseline releases*. Available at: <https://earth.esa.int/eogateway/instruments/aladin/processor-releases> [Accessed 2nd April 2022].
- ESA (2020–2022) *Aeolus balloon pass tool v1.1.1*. Available at: <https://eop-cfi.esa.int/index.php/applications/tools/command-line-tools-aeolus-balloon-pass>.
- Friedrich, L.S., McDonald, A.J., Bodeker, G.E., Cooper, K.E., Lewis, J. and Paterson, A.J. (2017) A comparison of loon balloon observations and stratospheric reanalysis products. *Atmospheric Chemistry and Physics*, 17, 855–866. <https://doi.org/10.5194/acp-17-855-2017>.
- Garrett, K., Liu, H., Ide, K., Hoffman, R.N. and Lukens, K.E. (2022) Optimization and impact assessment of Aeolus HLOS wind data assimilation in NOAA's global forecast system. *Quarterly Journal of the Royal Meteorological Society*, 148, 2703–2716. <https://doi.org/10.1002/qj.4331>.
- Haase, J., Alexander, M., Hertzog, A., Kalnajs, L., Deshler, T., Davis, S., Plougonven, R., Cocquerez, P. and Venel, S. (2018) Around the world in 84 days. *EOS*, 99. Available at: <https://eos.org/science-updates/around-the-world-in-84-days>.
- Haase, J. S., Alexander, M. J., Cocquerez, P., Davis, S. M., Deshler, T., Durr, G., Hauchecorne, A., Hertzog, A., Kalnajs, L., Plougonven, R., Ravetta, F. and Renard, J.-B. (2020) The first flights of the Strateole-2 technology demonstration campaign: observing the global equatorial tropopause with long-duration balloons. In *AGU Fall Meeting*, p. P050-14. Available at: <https://hal-insu.archives-ouvertes.fr/insu-03259189>.
- Helie, A., Wernham, D., Mason, G. and Straume, A.G. (2021) *AEOLUS-2 mission pre-development status*. In: Babu, S.R., Hélière, A. and Kimura, T. (Eds.) *Sensors, Systems, and Next-Generation Satellites XXV*, Vol. 11858. Bellingham, WA: International Society for Optics and Photonics, SPIE, pp. 36–43. <https://doi.org/10.1117/12.2599797>.
- Hertzog, A., Basdevant, C., Vial, F. and Mechoso, C. (2004) The accuracy of stratospheric analyses in the northern hemisphere inferred from long-duration balloon flights. *Quarterly Journal of the Royal Meteorological Society*, 130, 607–626. <https://doi.org/10.1256/qj.03.76>.
- Hertzog, A., Cocquerez, P., Guilbon, R., Valdivia, J.-N., Venel, S., Basdevant, C., Boccara, G., Bordereau, J., Briot, B., Vial, F., Cardonne, A., Ravissot, A. and Schmitt, É. (2007) *Stratéole/vorcore—long-duration, superpressure balloons to study the antarctic lower stratosphere during the 2005 winter*. *Journal of Atmospheric and Oceanic Technology*, 24, 2048–2061. <https://doi.org/10.1175/2007JTECHA948.1>.
- Hertzog, A. and Plougonven, R. (2021) *Stratéole-2: high-resolution observations of the tropical tropopause layer with long-duration balloons*. In: *EGU General Assembly Conference Abstracts*. EGU General Assembly. EGU21-7109. Available at: <https://ui.adsabs.harvard.edu/abs/2021EGUGA..23.7109H>.
- Horányi, A., Cardinali, C., Rennie, M. and Isaksen, L. (2015a) The assimilation of horizontal line-of-sight wind information into the ECMWF data assimilation and forecasting system. Part I: the assessment of wind impact. *Quarterly Journal of the Royal Meteorological Society*, 141, 1223–1232. <https://doi.org/10.1002/qj.2430>.
- Horányi, A., Cardinali, C., Rennie, M. and Isaksen, L. (2015b) The assimilation of horizontal line-of-sight wind information into the ECMWF data assimilation and forecasting system. Part II: the impact of degraded wind observations. *Quarterly Journal of the Royal Meteorological Society*, 141, 1233–1243. <https://doi.org/10.1002/qj.2551>.
- Houchi, K., Stoffelen, A., Marseille, G. and De Kloe, J. (2010) Comparison of wind and wind shear climatologies derived from high-resolution radiosondes and the ECMWF model. *Journal of Geophysical Research: Atmospheres*, 115, D22123. <https://doi.org/10.1029/2009JD013196>.
- Ingmann, P. and Straume, A. (2016) *ADM-Aeolus mission requirements document*. Centre ESRA-T. Available at: <https://earth.esa.int/eogateway/documents/20142/1564626/Aeolus-Mission-Requirements.pdf>.
- Laroche, S. and St-James, J. (2022) Impact of the Aeolus Level-2B horizontal line-of-sight winds in the environment and climate change Canada global forecast system. *Quarterly Journal of the Royal Meteorological Society*, 148, 2047–2062. <https://doi.org/10.1002/qj.4300>.
- Lux, O., Lemmerz, C., Weiler, F., Marksteiner, U., Witschas, B., Rahm, S., Geiß, A. and Reitebuch, O. (2020) Intercomparison of wind observations from the European Space Agency's Aeolus satellite mission and the Aladin airborne demonstrator. *Atmospheric Measurement Techniques*, 13, 2075–2097. <https://doi.org/10.5194/amt-13-2075-2020>.
- Marseille, G.-J., Stoffelen, A. and Barkmeijer, J. (2008) Impact assessment of prospective spaceborne Doppler wind lidar observation scenarios. *Tellus A: Dynamic Meteorology and Oceanography*, 60, 234–248. <https://doi.org/10.1111/j.1600-0870.2007.00289.x>.
- Martin, A., Weissmann, M., Reitebuch, O., Rennie, M., Geiß, A. and Cress, A. (2021) Validation of Aeolus winds using radiosonde observations and numerical weather prediction model equivalents. *Atmospheric Measurement Techniques*, 14, 2167–2183. <https://doi.org/10.5194/amt-14-2167-2021>.
- Spacenews. (2021) Google to shut down loon. Available at: <https://spacenews.com/google-to-shut-down-loon/> [Accessed 7th February 2022].
- Osprey, S.M. (2020) Autonomous balloons take flight with artificial intelligence. *Nature*, 588, 33–34. <https://www.nature.com/articles/d41586-020-03313-1>.
- Podglajen, A., Hertzog, A., Plougonven, R. and Žagar, N. (2014) Assessment of the accuracy of (re) analyses in the equatorial lower stratosphere. *Journal of Geophysical Research: Atmospheres*, 119, 11–166. <https://doi.org/10.1002/2014JD021849>.
- Pourret, V., Šavli, M., Mahfouf, J.-F., Raspaud, D., Doerenbecher, A., Bénichou, H. and Payan, C. (2021) Operational assimilation of Aeolus winds in the météo-France global NWP model Arpege. *Quarterly Journal of the Royal Meteorological Society*, 148, 2652–2671. <https://doi.org/10.1002/qj.4329>.

- Reitebuch, O. (2012) The spaceborne wind lidar mission ADM-Aeolus. In: Schumann, U. (Ed.) *Atmospheric Physics*. Berlin: Springer, pp. 487–507. https://doi.org/10.1007/978-3-642-30183-4_49.
- Reitebuch, O., Krisch, I., Lemmerz, C., Lux, O., Marksteiner, U., Masoumzadeh, N., Weiler, F., Witschas, B., Bracci, F., Meringer, M., Schmidt, K., Huber, D., Nikolaus, I., Fabre, F., Vaughan, M., Reissig, K., Dabas, A., Flament, T., Lacour, A., Mahfouf, J.-F., Šavli, M., Trapon, D., Abdalla, S., Isaksen, L., Rennie, M., Donovan, D., de Kloe, J., Marseille, G.-J., Stoffelen, A., Perron, G., Jupin-Langlois, S., Smeets, J., Veneziani, M., Bucci, S., Gostinich, G., Ehlers, F., Kanitz, T., Straume, A.-G., Wernham, D., von Bismarck, J., Bley, S., Fischer, P., De Laurentis, M. and Parrinello, T. (2020b) Assessment of Aeolus performance and bias correction—results from the Aeolus disc. In: *Aeolus Cal/Val and Science Workshop 2020*. Available at: https://elib.dlr.de/138648/1/Oliver_Reitebuch_Oral_Assessment-Aeolus-DISC.pdf.
- Reitebuch, O., Lemmerz, C., Lux, O., Marksteiner, U., Rahm, S., Weiler, F., Witschas, B., Meringer, M., Schmidt, K., Huber, D., Nikolaus, I., Geiß, A., Vaughan, M., Dabas, A., Flament, T., Stieglitz, H., Isaksen, L., Rennie, M., de Kloe, J., Marseille, G.-J., Stoffelen, A., Wernham, D., Kanitz, T., Straume, A.-G., Fehr, T., von Bismarck, J., Floberghagen, R. and Parrinello, T. (2020a) Initial assessment of the performance of the first wind lidar in space on Aeolus. In: *EPJ Web of Conferences*, vol. 237, p. 01010. <https://doi.org/10.1051/epjconf/202023701010>.
- Rennie, M. (2016) *Advanced monitoring of Aeolus winds*. ECMWF. Technical report TN16. Available at: <https://www.ecmwf.int/node/18014>.
- Rennie, M. and Isaksen, L. (2020) *The NWP impact of Aeolus Level-2B winds at ECMWF*. ECMWF Technical Memo. Technical report. <https://doi.org/10.21957/alift7mhr>.
- Rennie, M., Tan, D., Andersson, E., Poli, P., Dabas, A., De Kloe, J., Marseille, G.-J. and Stoffelen, A. (2020) Aeolus Level-2B algorithm theoretical basis document (mathematical description of the Aeolus Level-2B processor). Change, 3.40, 23-12. Available at: https://get.ecmwf.int/repository/test-data/Aeolus_L2Bp/v3.60/L2BP_Release_3_60_documents.tar.gz.
- Rennie, M.P., Isaksen, L., Weiler, F., de Kloe, J., Kanitz, T. and Reitebuch, O. (2021) The impact of Aeolus wind retrievals on ECMWF global weather forecasts. *Quarterly Journal of the Royal Meteorological Society*, 147, 3555–3586. <https://doi.org/10.1002/qj.4142>.
- Rhodes, B. and Candido, S. (2021) *Loon stratospheric sensor data*. Available at: <https://doi.org/10.5281/zenodo.5119968>.
- Ruppert, D. and Matteson, D.S. (2011) *Statistics and Data Analysis for Financial Engineering*, Vol. 13. New York, NY: Springer.
- Salonen, K., Cotton, J., Bormann, N. and Forsythe, M. (2012) Characterising AMV height assignment error by comparing best-fit pressure statistics from the met office and ECMWF system. In: *Proceedings of the 11th International Wind Workshop*, Auckland, pp. 20–24. Available at: https://www-cdn.eumetsat.int/files/2020-04/pdf_conf_p60_s5_06_salonen_v.pdf.
- Šavli, M., Pourret, V., Payan, C. and Mahfouf, J.-F. (2021) Sensitivity of Aeolus HLOS winds to temperature and pressure specification in the L2B processor. *Atmospheric Measurement Techniques*, 14, 4721–4736. <https://doi.org/10.5194/amt-14-4721-2021>.
- Šavli, M., Žagar, N. and Anderson, J. (2018) Assimilation of the horizontal line-of-sight winds with a mesoscale EnKF data assimilation system. *Quarterly Journal of the Royal Meteorological Society*, 144, 2133–2155. <https://doi.org/10.1002/qj.3323>.
- Stephan, C.C., Žagar, N. and Shepherd, T.G. (2021) Waves and coherent flows in the tropical atmosphere: new opportunities, old challenges. *Quarterly Journal of the Royal Meteorological Society*, 147, 2597–2624. <https://doi.org/10.1002/qj.4109>.
- Stoffelen, A., Pailleux, J., Källén, E., Vaughan, J.M., Isaksen, L., Flamant, P., Wergen, W., Andersson, E., Schyberg, H., Culoma, A., Meynart, R., Endemann, M. and Ingmann, P. (2005) The atmospheric dynamics mission for global wind field measurement. *Bulletin of the American Meteorological Society*, 86, 73–88. <https://doi.org/10.1175/BAMS-86-1-73>.
- Stoffelen, A., Reitebuch, O., Isaksen, L., v. Bismarck, J., Marksteiner, U., Weiler, F., Huber, D., Rennie, M., Dabas, A., Flament, T., Straume-Lindner, A. G., Kanitz, T., de Kloe, J., Marseille, G.-J. and van Zadelhoff, G.-J. (2019) Aeolus first results. In: *Joint EUMETSAT/AMS/NOAA Conference 2019*. Available at: <https://elib.dlr.de/127413/>.
- Straume, A.G., Rennie, M., Isaksen, L., de Kloe, J., Marseille, G.-J., Stoffelen, A., Flament, T., Stieglitz, H., Dabas, A., Huber, D., Reitebuch, O., Lemmerz, C., Lux, O., Marksteiner, U., Weiler, F., Witschas, B., Meringer, M., Schmidt, K., Nikolaus, I., Geiss, A., Flamant, P., Kanitz, T., Wernham, D., von Bismarck, J., Bley, S., Fehr, T., Floberghagen, R. and Parrinello, T. (2020) Esa's space-based doppler wind lidar mission Aeolus—first wind and aerosol product assessment results. In: *EPJ Web of Conferences*, 237, p. 01007. <https://doi.org/10.1051/epjconf/202023701007>.
- Tan, D.G., Andersson, E., Kloe, J.D., Marseille, G.-J., Stoffelen, A., Poli, P., Denneulin, M.-L., Dabas, A., Huber, D., Reitebuch, O., Flamant, P., Le Rille, O. and Nett, H. (2008) The ADM-Aeolus wind retrieval algorithms. *Tellus A: Dynamic Meteorology and Oceanography*, 60, 191–205. <https://doi.org/10.1111/j.1600-0870.2007.00285.x>.
- Velden, C.S. and Bedka, K.M. (2009) Identifying the uncertainty in determining satellite-derived atmospheric motion vector height attribution. *Journal of Applied Meteorology and Climatology*, 48, 450–463. <https://doi.org/10.1175/2008JAMC1957.1>.
- Vincent, R. and Hertzog, A. (2014) The response of superpressure balloons to gravity wave motions. *Atmospheric Measurement Techniques*, 7, 1043–1055.
- Weiler, F., Rennie, M., Kanitz, T., Isaksen, L., Checa, E., de Kloe, J., Okande, N. and Reitebuch, O. (2021) Correction of wind bias for the lidar on-board Aeolus using telescope temperatures. *Atmospheric Measurement Techniques*, 14, 7167–7185.
- Wergen, W. (2011) *Dealing with larger than average turbulence in ADM-Aeolus observations*. ESA. Technical report. Available at: https://www.aeolus.esa.int/confluence/pages/viewpage.action?pageId=3509%5746&preview=%2F35095746%2F35095825%2F2012+Effect+Turbulence+WW_report_rev1.1.pdf.
- Witschas, B., Lemmerz, C., Geiß, A., Lux, O., Marksteiner, U., Rahm, S., Reitebuch, O. and Weiler, F. (2020) First validation of Aeolus wind observations by airborne doppler wind lidar measurements. *Atmospheric Measurement Techniques*, 13, 2381–2396. <https://doi.org/10.5194/amt-13-2381-2020>.

- Žagar, N. (2017) A global perspective of the limits of prediction skill of NWP models. *Tellus A: Dynamic Meteorology and Oceanography*, 69, 1317573. <https://doi.org/10.1080/16000870.2017.1317573>.
- Žagar, N., Isaksen, L., Tan, D. and Tribbia, J. (2013) Balance properties of the short-range forecast errors in the ECMWF 4D-Var ensemble. *Quarterly Journal of the Royal Meteorological Society*, 139, 1229–1238. <https://doi.org/10.1002/qj.2033>.
- Žagar, N., Rennie, M. and Isaksen, L. (2021) Uncertainties in kelvin waves in ECMWF analyses and forecasts: insights from Aeolus observing system experiments. *Geophysical Research Letters*, 48, e2021GL094716. <https://doi.org/10.1029/2021GL094716>.

How to cite this article: Bley, S., Rennie, M., Žagar, N., Pinol Sole, M., Straume, A.G., Antifaev, J. *et al.* (2022) Validation of the Aeolus L2B Rayleigh winds and ECMWF short-range forecasts in the upper troposphere and lower stratosphere using Loon super pressure balloon observations. *Quarterly Journal of the Royal Meteorological Society*, 148(749), 3852–3868. Available from: <https://doi.org/10.1002/qj.4391>